Journal of Sound and Vibration 459 (2019) 114843

Contents lists available at ScienceDirect

Journal of Sound and Vibration

journal homepage: www.elsevier.com/locate/jsvi

Geometric phase invariance in spatiotemporal modulated elastic system

M. Arif Hasan*, Lazaro Calderin, Pierre Lucas, Keith Runge, Pierre A. Deymier

Department of Materials Science and Engineering, University of Arizona, Tucson, AZ, 85721, USA

ARTICLE INFO

Article history:
Received 8 January 2019
Received in revised form 22 May 2019
Accepted 6 July 2019
Available online 10 July 2019
Handling Editor: W. Zhu

Keywords:
Geometric phase
Invariance
Modulation
Elastic system

ABSTRACT

We study the topological characteristics of elastic waves in a one-dimensional mass and spring elastic superlattice that exhibits non-reciprocal elastic wave propagation due to extrinsic application of a single sinusoidal spatiotemporal modulation of its spring stiffness. We employ a computational procedure to generate the band structure, traveling modes' amplitudes and phases, and subsequently the geometric phases to characterize the global vibrational behavior of the system and its topological character. The elastic superlattice demonstrates the notion of non-conventional band structure, where hybridization gaps arise as bands appear and cross for certain wavenumber values. We estimate these hybridization points using multiple time scale perturbation theory for low modulation velocity. At the hybridization points, both the theoretical and numerical analyses display a discontinuity in the traveling modes' amplitudes. Consequently, we find a multiple of π, sometimes zero, geometric phase value in the spatiotemporal modulated elastic system, if the unit cell has inversion symmetry as imposed by the values of the spring constant at the initial time. The temporal modulation, which creates hybridization gaps, changes the nature of the geometric phase from a closed loop geometric phase when the modulation is only spatial, to an open loop geometric phase. This open loop geometric phase is invariant to the temporal modulation.

© 2019 Elsevier Ltd. All rights reserved.

1. Introduction

The emergence of a new science of sound accounts not only for spectral and refractive characteristics of waves but also the amplitude and phase of the waves [1], which under symmetry breaking conditions may lead to non-conventional topology. In phononic crystals, symmetry breaking is linked to constraints on the topological form of acoustic wave functions. For instance, in the context of topology, for the well-known driven damped oscillator, the amplitude of the wave function has properties isomorphic to the evolution of a field of parallel vectors tangent to a strip-like manifold and perpendicular to the length of the strip. The direction along the length of the strip represents frequency space and the strip has to exhibit a torsion (vectors in the vector field change orientation) at the oscillator resonant frequency as the amplitude changes sign as one crosses the resonance (i.e., the amplitude accumulates a π-phase shift). Dissipation aside, one of the most central elements to symmetry breaking and topology of elastic waves, is dispersion. A simple, linear one-dimensional (1D) harmonic monoatomic

* Corresponding author.
E-mail addresses: mdhasan@email.arizona.edu (M.A. Hasan), lcalderin@email.arizona.edu (L. Calderin), pierre@email.arizona.edu (P. Lucas), krunge@email.arizona.edu (K. Runge), deymier@email.arizona.edu (P.A. Deymier).

https://doi.org/10.1016/j.jsv.2019.07.009
0022-460X/© 2019 Elsevier Ltd. All rights reserved.

chain is a dispersive system, but one that obeys time-reversal symmetry and supports elastic waves with conventional topology in wave vector space. Perturbing the 1D harmonic chain through linear or nonlinear coupling may create resonant phonon modes that are dispersive, but whose amplitude may depend on the frequency and wave vector. In this case, the interplay between the coupling and dispersion of the system may lead to symmetry breaking conditions and therefore non-conventional elastic wave topology. Examples for the breaking of symmetries including time-reversal symmetry, chiral symmetry, and particle-hole symmetry [1]. An alternative realization of intrinsic parity symmetry breaking which is comprised of a one-dimensional (1D) harmonic crystal with masses attached to a rigid substrate through harmonic springs has been shown to possess a spin-like topology that can be described by a Dirac-like equation [2,3]. Complementing intrinsic symmetry breaking are extrinsic topological phononic structures which have been created using a periodic spatial modulation of the stiffness of a 1D elastic medium such that its directed temporal evolution breaks both time-reversal and parity symmetries [4–10].

The development of acoustic analogues of quantum phenomena offers additional perspectives for applications and technological developments of the new science of sound. Within a wide range of quantum phenomena, the Berry phase or, more generally, the geometric phase has considerable observable impact. In fact, it can also appear in classical systems as discovered by Hannay in 1985 [11]. The concept of geometric phase has implications in several branches of physics and has found applications in molecular systems [12], in cold atoms [13,14], photonic systems [15,16], and also in acoustic systems [17–20]. Elastic structures have been shown recently to possess non-conventional topology by breaking time-reversal symmetry (time-dependent superlattice) through addition of energy from the outside [4,5,21–26].

One can define the geometric phase as the holonomy of phase that is purely of geometrical origin, which became popular after the discovery of the Berry phase [27]. The Berry phase is defined on the interval between 0 and 2π, i.e., it is reported modulo 2π, while Berry phases of 0 and π are frequently linked to trivial and non-trivial topologies. While the Berry phase was originally investigated for periodic, or cyclic, systems that varied slowly, adiabatically, Samuel and Bhandari showed that neither of these conditions is required for the computation of a geometrical phase [28]. In particular, one can compute an open path geometric phase for the non-periodic system that is consistent with the Berry phase for a periodic system.

We have carried out the calculation of geometric phases for band structures arising from a one dimensional (1D) mass and spring elastic superlattice with a spatial modulation of stiffness [29]. It is observed that the symmetry of the modulation of stiffness with respect to inversion dictates whether the bands' Berry phases were 0, π, or some other value. In the current manuscript, we investigate the effect on geometric phases that arises from adding a temporal modulation to the spatial modulations considered in the previous study. In particular, we consider a moving spatial modulation with a fixed velocity along a 1D elastic superlattice. Applying computational tools developed in the case of the spatial modulation, we note that the geometric phase of the first two fundamental bands does not change due to the temporal modulation. The temporal modulation does open gaps in the band structure, however, and the geometric phase becomes an open path geometric phase. These numerical results are explained within the context of multiple time scale perturbation theory.

The structure of the paper is the following: in Section 2 we present a 1D mass and spring elastic superlattice subjected to spatiotemporal modulations of the stiffness. In Section 3, we illustrate the computational tool for the spectral analysis of amplitudes and phases, and a theoretical analysis within the framework of method of multiple time scales. In Section 4, we present results for time-dependent superlattice and compare with time-independent superlattice to demonstrate the invariance of the geometric phase. We draw conclusions in Section 5.

2. Mass and spring model

We seek to explore the topological characteristics of elastic waves in a 1D mass and spring elastic superlattice (Fig. 1). For a mass and spring system with a total of $N_m N_c$ identical masses, where N_m is the number of masses in a single unit cell and N_c is the total number of unit cells, the equations of motion are:

$$m\ddot{u}_{n,N_i}(t) = \beta_{n-1}(t)\left[u_{n-1,N_i}(t) - u_{n,N_i}(t)\right] - \beta_n(t)\left[u_{n,N_i}(t) - u_{n+1,N_i}(t)\right] \tag{1}$$

where $u_{0,N_i} = u_{N_m,N_i-1}$; $u_{0,1} = u_{N_m,N_c}$; $u_{N_m+1,N_i} = u_{1,N_i+1}$; $u_{N_m+1,N_c} = u_{1,1}$; $\beta_0 = \beta_{N_m}$. In Eq. (1), m is the mass, β_n is the force constant of the $n-th$ spring, t is time, and $u_{n,N_i}(t)$ is the displacement from equilibrium as a function of time t of the $n-th$ mass in the N_i-th unit cell of the chain, respectively. We use Born-von Karman periodic boundary conditions for which

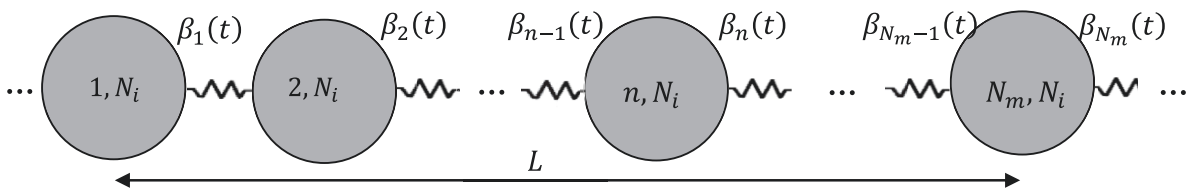

Fig. 1. Schematic illustration of a 1D chain comprised of masses and springs with spatiotemporal modulations of the spring stiffness.

$e^{ikLN_c} = 1$, where L is the unit cell parameter, and k is the wave number. In the first Brillouin zone, kL is limited to the interval $-\pi$ to π with a spacing of $2\pi/N_c$. For this study, we consider a four mass unit cell for comparison with results from the static spatial modulation of stiffness.

The spring constants have a modulation in time and space that is sinusoidal so that:

$$\beta_n(t) = \beta_0 \pm \Delta\beta \sin(k_m x_n - \omega_m t) \tag{2}$$

In Eq. (2), β_0 is the unmodulated spring constant, $\Delta\beta$ is the modulation amplitude, and k_m and ω_m are the propagation wave number and the angular frequency of the modulation, respectively. Therefore, the mass and spring system can be described as the assembly of unit cells of spatial modulation period being $\lambda_m = 2\pi/k_m = L = N_m a$, where a is the inter-mass spacing and $N_m = 4$ is the number of masses per unit cell. As such,

$$\beta_n(t) = \beta_0 \pm \Delta\beta \sin\left(\frac{2\pi}{L}(x_n - V_m t)\right), \tag{3}$$

where $V_m = \omega_m/k_m = \omega_m L/2\pi$ is the speed of the modulation. For the sake of simplicity, we define the spring constant modulation of $\beta_n(t) = \beta_0 + \Delta\beta \sin(2\pi(x_n - V_m t)/L)$ type as β_n^+ and $\beta_n(t) = \beta_0 - \Delta\beta \sin(2\pi(x_n - V_m t)/L)$ type as β_n^-. The arrangements of the springs constants β_n^+ and β_n^- are related to each other by a change in origin of the unit cell from mass 1 to mass $(N_m/2 + 1)$ i.e., by shifting the origin to the left/right by half of the unit cell parameter L. In the modulated medium, due to the repetition of the unit cell, both stable and unstable interactions can occur [30]. To have a stable interaction that is associated with frequency conversion effects [30], we limit the phase velocity of the modulation to be less than that of the signal in the modulated medium, i.e. $V_m < c_0$, where $c_0 = \sqrt{E/\rho}$ is the phase velocity of the longitudinal wave in the medium, E is the longitudinal elastic constant, and ρ is the density. We consider the medium to be composed of Ge-Se chalcogenide glass of composition $GeSe_4$ [31] with $E = 13.8$ GPa and $\rho = 4361$ kg/m^3. Therefore the sound velocity is $c_0 = 1780$ m/s. We also impose the physical restriction of the relative modulation amplitude such that $\Delta\beta/\beta_0 < 1$ i.e., the spring constant must remain positive.

3. Methods

We investigate the vibrational properties of the time-dependent elastic superlattice both computationally and using multiple time scales perturbation theory.

3.1. Computational method: spectral analysis of amplitudes and phases (SAAP)

The Spectral Analysis of Amplitudes and Phases (SAAP) method [29] is employed to computationally generate the band structure, traveling modes' amplitudes and phases, and subsequently the Berry connections and geometric phases associated with the bands of an elastic periodic superlattice, as a characterization of the global vibrational behavior of the elastic system and its topological character. Traditional theoretical approaches such as the eigen value/vector approach are limited to linear systems, however the SAAP method which is directly related to the dynamics of the system can be applied to either linear or nonlinear systems. The SAAP method entails the use of molecular dynamics (MD) simulation twice with differing initial conditions. The choice of initial conditions for the simulations is essential to compute both the band structures and phases. For the 1st MD, we choose the initial conditions as $u_{n,N_i}(0) = \cos(kN_iL)$ and $\dot{u}_{n,N_i}(0) = 0$. After each MD run for a specific wave number k, the frequency spectrum is found by the temporal integral of the displacement $u_{n,N_i}(t)$

$$\tilde{u}_{n,N_i}(\omega) = \frac{1}{\tau_0}\int_0^{\tau_0} u_{n,N_i}(t) e^{-i\omega t} dt \tag{4}$$

In Eq. (4), τ_0 is the total time of the MD run for which the displacements are tabulated. Eq. (4) is like a Fourier transform whose peak positions define the frequencies for the given value of k. Since, multiple frequencies can be supported for a single wave number k, we denote the frequencies as $\omega_j(k)$ which refers to the jth lowest frequency the system supports for wave number k. Once $\omega_j(k)$ is known, we calculate the elastic wave amplitudes and phases using another set of MD simulations with new initial conditions $u_{n,N_i}(0) = \cos(kN_iL)$ and $\dot{u}_{n,N_i}(0) = -\omega_j(k)\sin(kN_iL)$. This new set of initial conditions now sets the values of the velocity to those prescribed by the computed band structure. We emphasize here that one has to use specific traveling elastic wave initial conditions, instead of random initial conditions, to obtain the amplitudes and then phases, since random initial conditions add or subtract a constant value to the phase. After the second set of MD simulation, we project the calculated displacement $u_{n,N_i}(t)$ with wave vector k and frequency $\omega_j(k)$ onto plane waves to calculate the complex amplitude $A_{nj}(k)$ as

$$A_{n,j}(k) = \frac{1}{N_c}\sum_{N_i=1}^{N_c}\frac{1}{\tau_0}\int_0^{\tau_0} u_{n,N_i}(t)e^{-ikN_iL}e^{-i\omega_j(k)t}dt, \tag{5}$$

and the elastic band structure is generated as

$$|A_j(k,\omega_j(k))| = \left|\frac{1}{N_m}\sum_{n=1}^{N_m}A_{n,j}(k)\right| \tag{6}$$

Finally, the phase of the complex amplitude is given by

$$\phi_{n,j}(k) = angle\ [A_{n,j}(k)]; \tag{7}$$

where

$$\text{angle }(z) = \begin{cases} \text{atan}\left(\dfrac{\text{Im}(z)}{\text{Re}(z)}\right) + \pi, if\ \ \text{sign}(\text{Re}(z)) < 0 \text{ and } \text{sign}(\text{Im}(z)) > 0 \\ \text{atan}\left(\dfrac{\text{Im}(z)}{\text{Re}(z)}\right) - \pi, \text{if}\ \ \text{sign}(\text{Re}(z)) < 0 \text{ and } \text{sign}(\text{Im}(z)) < 0. \end{cases}$$

Note that the phase of z is defined on the interval $-\pi$ to π.

A further characterization of the behavior of the amplitudes is realized by the Berry connection for a particular band of the band structure. When the system contains a finite number of unit cell, N_C, the Brillouin zone is discretized and the Berry connection is given by Ref. [32].

$$BC_j(k) = \sum_{n=1}^{N_m}\tilde{A}^*_{n,j}(k)\tilde{A}_{n,j}(k+\Delta k), \tag{8}$$

In Eq. (8), $BC_j(k)$ is the Berry connection value for a discrete wave number (k) of band j and $\Delta kL = 2\pi/N_C$, and $\tilde{A}_{n,j}(k)$ is the normalized complex amplitude for the *n-th* mass in a unit cell on band j and is calculated as

$$\tilde{A}_{n,j}(k) = \frac{A_{n,j}(k)}{\sqrt{\sum_{n=1}^{N_m}|A_{n,j}(k)|^2}} \tag{9}$$

The $\tilde{A}_{n,j}(k)$ with $n \in [1, N_m]$ represent the complex *n-th* components of a unit vector in a N_m dimensional complex space. This normalized amplitude unit vector (n.b., the normalization is for the full vector) can be defined as:

$$\vec{\tilde{A}} = (\tilde{A}_{1,j}(k), \tilde{A}_{2,j}(k), \ldots, \tilde{A}_{N_m,j}(k)) \tag{10}$$

This amplitude unit vector evolves along some parametric curve as k is varied. The Berry connection characterizes the variation in orientation of the unit vector along some path in the complex space of amplitudes parametrized by k. Summing the Berry connection for the possible k values of some specific band over a path in k-space defined by the first Brillouin zone, gives the geometric phase. Therefore, the geometric phase ϕ_G of band j is then defined as [32].

$$\phi_{G,j} = -Im\left\{\ln\left[\prod_{i=1}^{N_c-1}BC_j(k_i)\right]\right\} mod\ 2\pi \tag{11}$$

In Eq. (11), Im takes the imaginary part of its argument. For infinite systems or continuous k, a differential form of the above expression is used [27]. The geometric phase that characterizes the property of bulk bands in periodic systems is known as the Zak phase [33], whereas Berry introduced the general concept of geometric phase earlier [27]. We use the term *geometric phase* for which the summation of Eq. (11) (or the line integral for the continuous system) is evaluated over an open path in k space, and we reserve the name of *Berry phase* for which the summation of Eq. (11) is evaluated along an arbitrary closed path in a parameter space. This is because the calculation of Berry phase is conditioned by the existence of a closed path in the k-space with the amplitudes or projections $\tilde{A}_{n,j}(k)$ being periodic in k space. Hence, for the calculation of Berry phase, $\tilde{A}_{n,j}(\pi/L)$ is taken to be same as $\tilde{A}_{n,j}(-\pi/L)$. Finally, the evolution of the amplitude unit vector $\vec{\tilde{A}}$ in the N_m dimensional space parametrized by the wave number k generates a manifold. The geometric phase is the net phase accumulated by the

amplitude unit vector over the entire manifold for a specified path. That is to say, the geometric phase characterizes the topology of the manifold. Therefore, the SAAP method is a useful tool to explore the topological characteristics of elastic waves in elastic structures. As we have seen above, in the SAAP method Newton's equations of motion are solved as a function of time via a molecular dynamics approach and the solutions are projected on to planes waves, which allows the extraction of the amplitudes including their phases. While in the current manuscript we test the SAAP computational tool on simple mass and spring models, the method can be applied to continuous systems including rods, beams and plates.

3.2. Theoretical study: method of multiple time scales

In Refs. [4,5] a multiple time scale perturbation theory [34] is used to study the time-dependent elastic superlattice in the long wavelength limit. Here, we summarize the analysis that will provide insight into the origin of the features discussed in Section 4. The displacement field $u(x,t)$ is written as a second order power series [4].

$$u(k+g,\tau_0,\tau_1,\tau_2) = u_0(k+g,\tau_0,\tau_1,\tau_2) + \varepsilon u_1(k+g,\tau_0,\tau_1,\tau_2) + \varepsilon^2 u_2(k+g,\tau_0,\tau_1,\tau_2), \tag{12}$$

where ε is a small perturbation parameter that is a measure of the magnitude of the modulation and $g = \frac{2\pi}{L}m$ with m being a positive or negative number. Here, u_i with $i = 0, 1, 2$ are the displacement functions expressed to zeroth-order, first-order, and second-order in the perturbation. The single time variable, t, is replaced by three variables representing different time scales: $\tau_0 = t, \tau_1 = \varepsilon t$, and $\tau_2 = \varepsilon^2 t$. The zeroth-order equation in ε represents propagation of an elastic wave in a homogeneous medium with the eigenvalue $\omega_0 = c_0(k+g)$. The solution to the first-order in ε is

$$\begin{aligned} u_1(k+g,\tau_0,\tau_2) = a_1(k+g,\tau_2)e^{i\omega_0(k+g)\tau_0} &+ i\frac{f(k+g-k_m)a_0(k+g-k_m,\tau_2)}{\omega_0^2(k+g) - [\omega_0(k+g-k_m)+\omega_m]^2}e^{i[\omega_0(k+g-k_m)+\omega_m]\tau_0} \\ &+ i\frac{f(k+g+k_m)a_0(k+g+k_m,\tau_2)}{\omega_0^2(k+g) - [\omega_0(k+g+k_m)-\omega_m]^2}e^{i[\omega_0(k+g+k_m)-\omega_m]\tau_0}, \end{aligned} \tag{13}$$

where $f(x) = xk_m + x^2$ and $h(x) = xk_m - x^2$. The zeroth- and first-order solutions give the positions of the hybridization gaps, k_{gap} (vide infra).

4. Results and discussion

4.1. Numerical results

We proceed to do the spectral analysis of elastic wave amplitudes and phases when the modulation velocity (V_m) is 350 m/s and for both β_n^+ and β_n^- modulation types. Fig. 2 shows the band structure of the spatiotemporal modulated elastic superlattice, calculated using Eq. (6). The spectrum $\omega_j(k)$ and hence the band structure remains invariant regardless of β_n^+ or β_n^- modulation type. Fig. 2 shows the directional band gaps i.e., opening of band gaps on only one side of the Brillouin zone, as previously observed by other researchers [4,5,7,8,35,36]. The location of the gaps can be tuned by changing the modulation speed [7].

The band structure of the time-dependent superlattice contains a series of frequency shifted bands (see Fig. 2). The frequency shift amounts to multiples of ω_m, which is independent of the speed of wave in the propagating medium if $V_m < c_0$ (unlike time-dependent photonic and phononic crystals [37,38]). The intensity of these bands decreases as the shift in frequency increases. Between the frequency shifted bands and the prior bands of the static modulation, hybridization gaps form

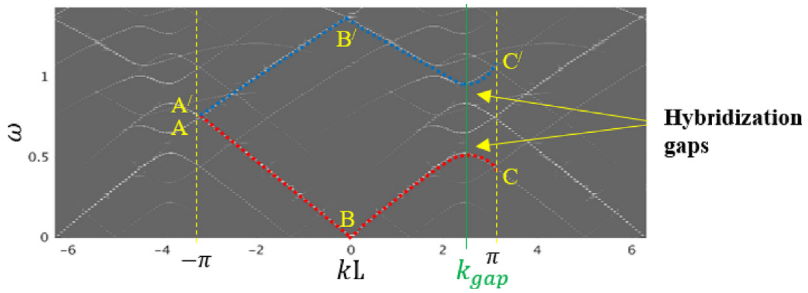

Fig. 2. Elastic wave band structure resulting from a moving periodic sinusoidal modulation with a modulation velocity of $V_m = 350\ m/s$. Red (blue) dotted line shows the 1st (2nd) fundamental branch below (above) the 1st (2nd) hybridization gap. Here, both axes are in units of radians, obtained by multiplying wave number by L and frequency by $\sqrt{m/\beta_0}$. System parameters: $m = 4.361 \times 10^{-9}$ kg, $a = 0.1$mm, $\beta_0 = 1380$kN/m, $\Delta\beta/\beta_0 = 1/3$, $N_c = 96$, and $N_m = 4$. (For interpretation of the references to colour in this figure legend, the reader is referred to the Web version of this article.)

at k_{gap} [5]. We define the band below the first hybridization gap as the 1st fundamental branch (FFB), and the band above the second hybridization gap as the 2nd fundamental branch (SFB). The path for the FFB (SFB) starts from A (A$^{/}$) and goes through point B (B$^{/}$) and ends at point C (C$^{/}$), as shown in Fig. 2 by the red (FFB) and blue (SFB) dotted lines. We denote the frequencies and amplitudes associated with the fundamental branches as $\omega_p(k)$ and $A_{n,p}(k)$, where p labels the fundamental branches. We wish to characterize the behavior of the amplitudes of these two fundamental branches by the Berry connection and geometric phase.

Figs. 3 and 4 show the real and imaginary components of the normalized complex amplitudes, $\tilde{A}_{n,p}(k)$. Fig. 3 (Fig. 4) shows the complex amplitudes of each mass n and each fundamental branch p for β_n^+ (β_n^-) modulation type. For β_n^+ modulation, we

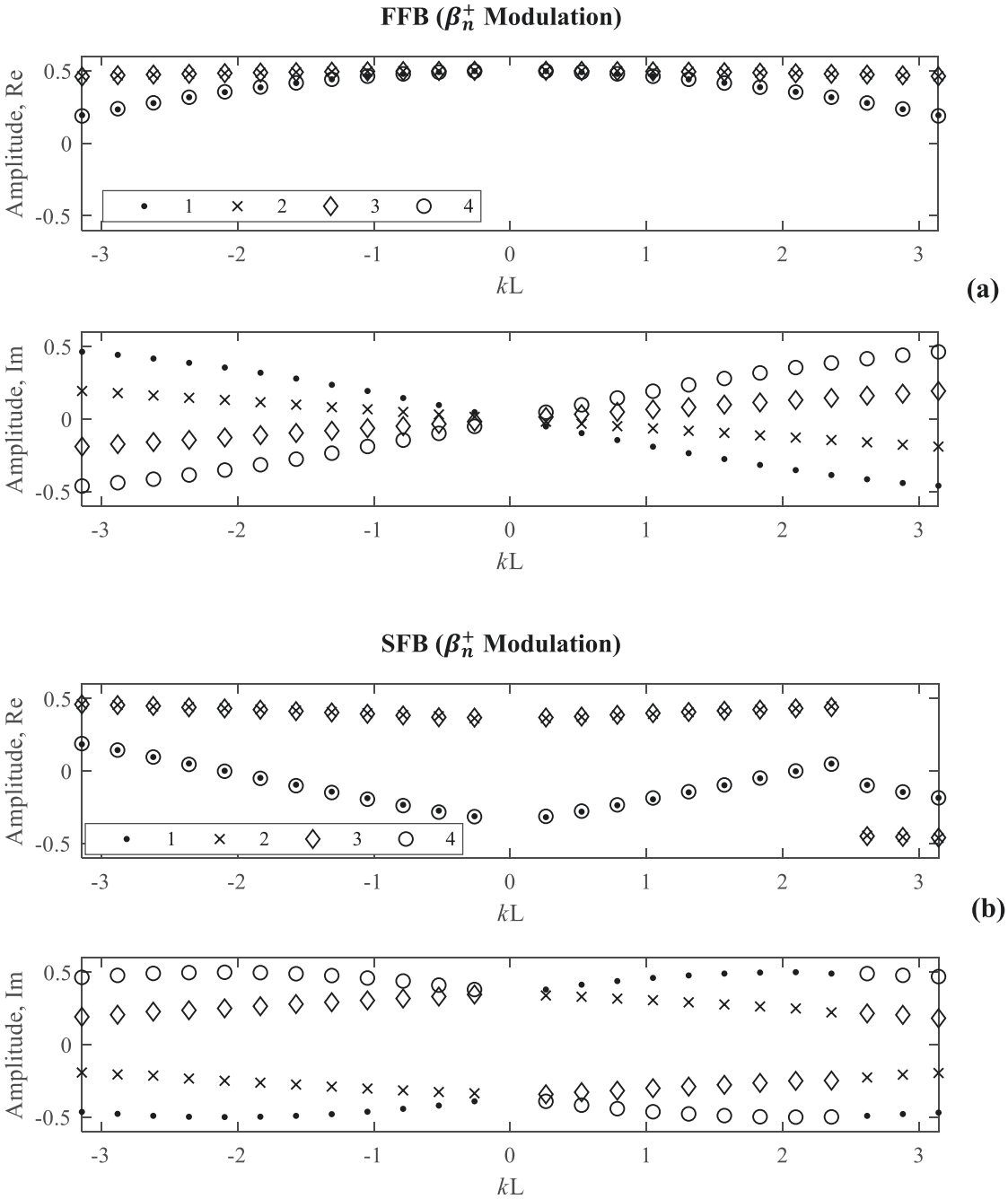

Fig. 3. Numerically calculated normalized complex amplitudes at the (a) FFB, and (b) SFB of masses 1, 2, 3, and 4 for the β_n^+ modulation. The system is composed of 24 unit cells.

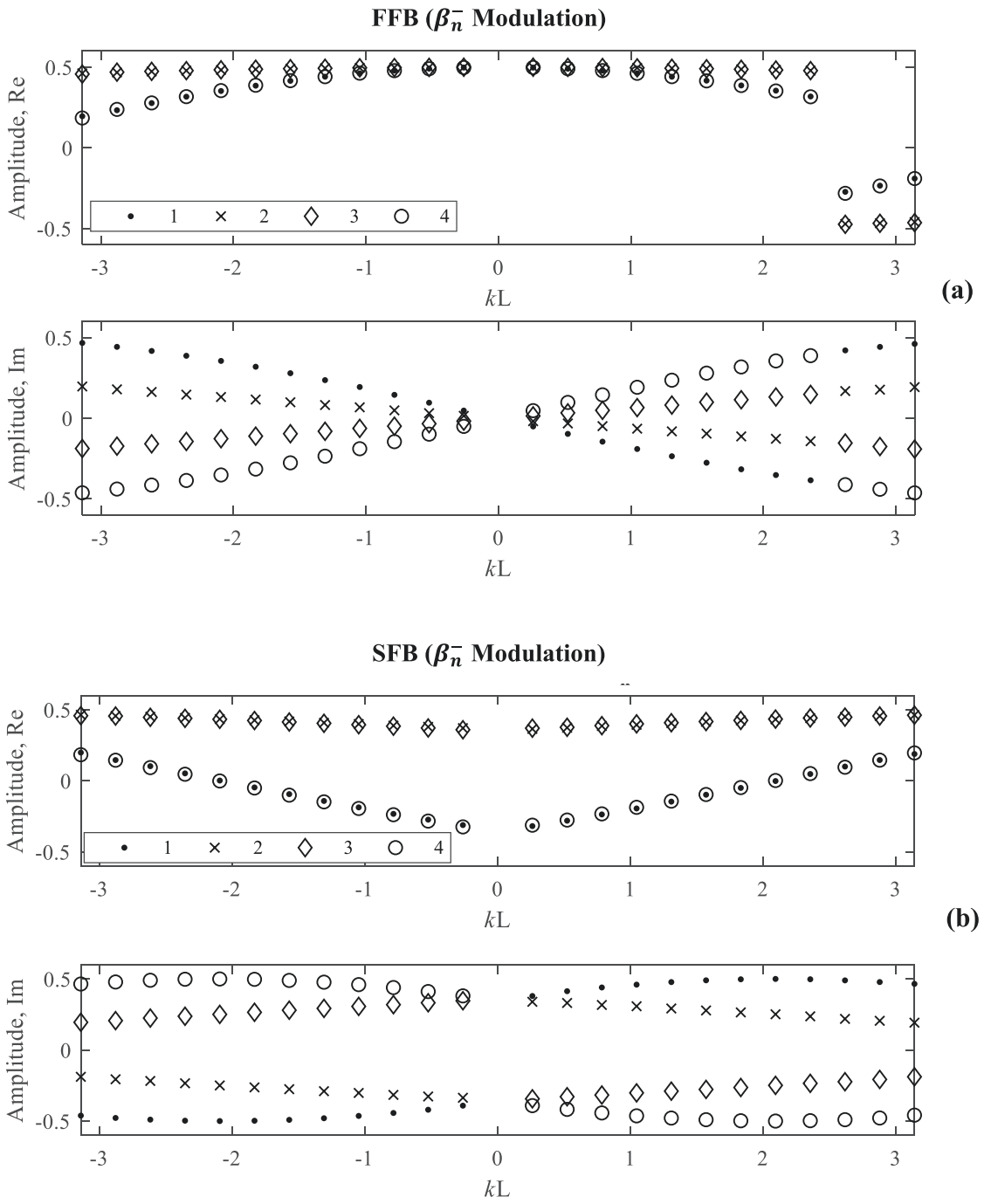

Fig. 4. Numerically calculated normalized complex amplitudes at the (a) FFB, and (b) SFB of masses 1, 2, 3, and 4 for the β_n^- modulation. The system is composed of 24 unit cells.

note from Fig. 3a that the real components of the FFB amplitude is an even function of k and the imaginary components is an odd function i.e., $\tilde{A}_{n,p}(k) = \tilde{A}^*_{n,p}(-k)$. However, for the SFB (Fig. 3b) we find $\tilde{A}_{n,p}(k) = \tilde{A}^*_{n,p}(-k)$ until k_{gap}, and $\tilde{A}_{n,p}(k) = -\tilde{A}^*_{n,p}(-k)$ after k_{gap} where there is a discontinuity. The discontinuity at k_{gap} leads to a change in sign of the real and imaginary components of the amplitudes. On the SFB, there is also a discontinuity for the imaginary components at $k = 0$, as well as, at k_{gap}. Therefore, for β_n^+ modulation type we observe either zero or two discontinuities for the imaginary components of the complex amplitudes.

Fig. 4 displays the same information about the real and imaginary components of the complex amplitudes for the β_n^- modulation.Unlike the β_n^+ modulation, for the β_n^- modulation, we observe a single discontinuity for the imaginary components of the amplitudes either at k_{gap} (FFB, see Fig. 4a) or at $k = 0$ (SFB, see Fig. 4b). As will discuss below, these discontinuities lead to a geometric phase value of either 0 or π. For both modulations, we also note that if there is a discontinuity at k_{gap} of the FFB amplitudes, there is no discontinuity at k_{gap} of the SFB amplitudes, and vice versa. Further, for a particular fundamental branch, if there is a discontinuity at k_{gap} for β_n^+ modulation, there is no discontinuity at k_{gap} for β_n^- modulation, and vice versa. Using SAAP tool, we can numerically estimate k_{gap}.

From Figs. 3 and 4 we also note that the real components of the complex amplitudes are equal for masses 1 and 4, and masses 2 and 3, and that the imaginary components of the amplitudes are equal but of opposite signs, so that for each of the fundamental branches we find $\tilde{A}_{1,p}(k) = \tilde{A}^*_{4,p}(k)$ and $\tilde{A}_{2,p}(k) = \tilde{A}^*_{3,p}(k)$. Fig. 5 shows the impact of these relations in terms of the phase values for masses 1 and 4, and masses 2 and 3 i.e., $\phi_{1,p}(k) = -\phi_{4,p}(k)$ and $\phi_{2,p}(k) = -\phi_{3,p}(k)$. This relationship is similar to that seen for the static system where it arises from the inversion symmetry of the elastic superlattice [29]. At the initial time, we have $\beta_1(0) = \beta_3(0)$ and hence mass 1 is connected with springs $\beta_1(0)$ and $\beta_4(0)$ to its right and left, and mass 4 is connected with springs $\beta_4(0)$ and $\beta_1(0)$ to its right and left. From Fig. 5, we also observe that the phase value is an odd function of wave number such that $\phi_{n,p}(k) = -\phi_{n,p}(-k)$ if there is no discontinuity at k_{gap}. If there is a discontinuity at k_{gap}, we find $\phi_{n,p}(k) = -\phi_{n,p}(-k)$ before k_{gap} and $\phi_{n,p}(k) = -\phi_{n,p}(-k) + \pi$ after k_{gap}.

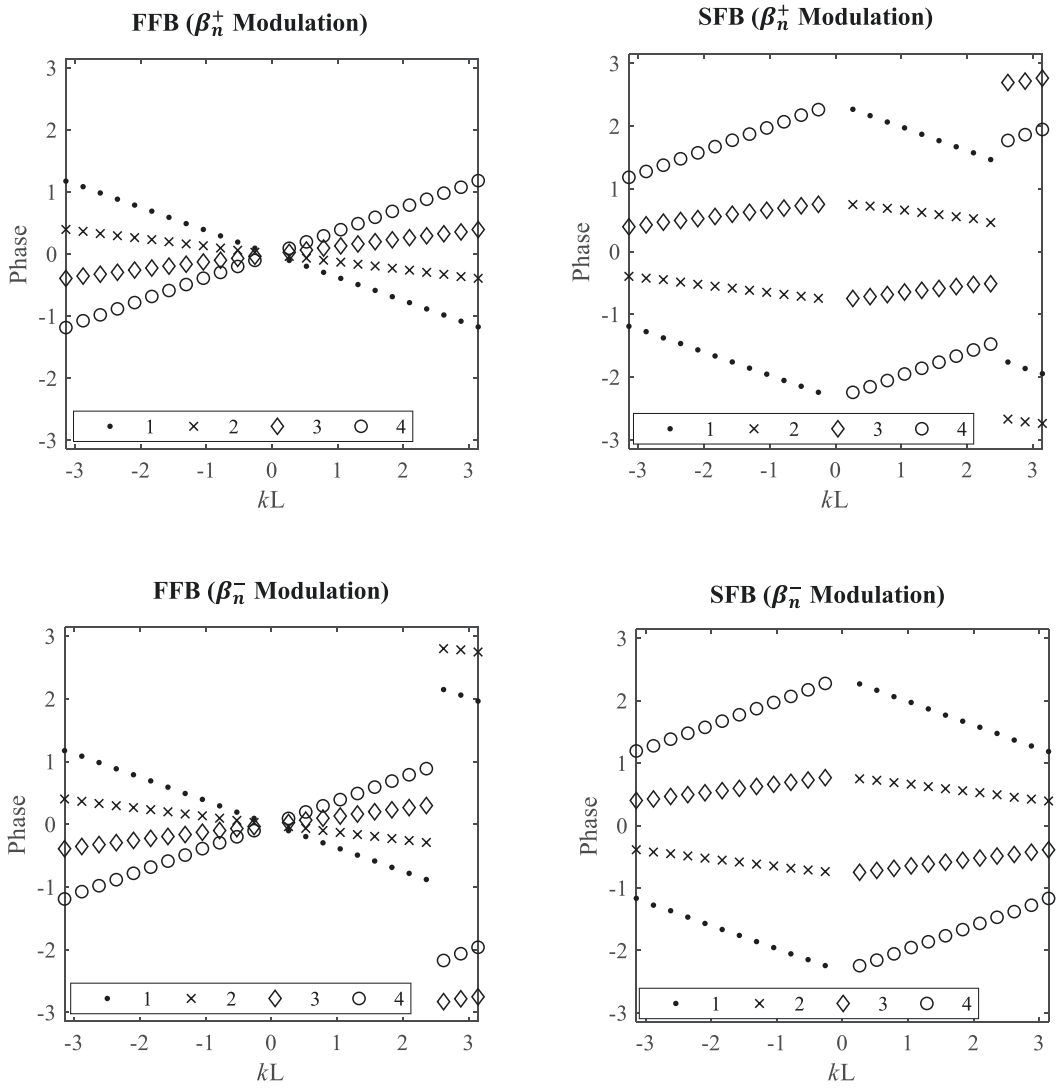

Fig. 5. Numerically calculated phase values of each mass n at each fundamental branches and for both modulations. The system is composed of 24 unit cells.

Using Eq. (8) of the Berry connection, we have for each fundamental branch:

$$BC_p(k) = \sum_{n=1}^{N_m} \tilde{A}^*_{n,p}(k)\tilde{A}_{n,p}(k+\Delta k) = \left\{\tilde{A}^*_{1,p}(k)\tilde{A}_{1,p}(k+\Delta k)\right\} + \left\{\tilde{A}^*_{1,p}(k)\tilde{A}_{1,p}(k+\Delta k)\right\}^* + \left\{\tilde{A}^*_{2,p}(k)\tilde{A}_{2,p}(k+\Delta k)\right\} + \left\{\tilde{A}^*_{2,p}(k)\tilde{A}_{2,p}(k+\Delta k)\right\}^*,$$

since at each fundamental branch we observed $\tilde{A}_{1,p}(k) = \tilde{A}^*_{4,p}(k)$ and $\tilde{A}_{2,p}(k) = \tilde{A}^*_{3,p}(k)$, regardless of the modulation. Therefore, $BC_p(k)$ given by the above equation is purely real with either positive or negative values and therefore a geometric phase of either 0 or π. In Fig. 6, we plot the Berry connection values on each fundamental branch and for both modulations and note that the connections are real. Using Eq. (11), we find that the geometric phase value is 0 for each fundamental branch for β_n^+ modulation and π for β_n^- modulation.

For a sinusoidal spatiotemporal modulated elastic superlattice, we find a multiple of π (either 0 or π) geometric phase values. We also observe that multiple of π geometric phase values are conditioned by the selection of the origin of the unit cell, i.e., the geometric phase value of 0 corresponds to β_n^+ modulation and π for β_n^- modulation. For the case of static only spatial modulation, we also note that the geometric phase values are the same for the β_n^+ modulation (that is, 0) and the β_n^- modulation (that is, π). In summary, the temporal modulation does not change the value of the geometric phase for either modulation, however, the path in k space goes from being closed in the static case i.e., $\omega_k\left(-\frac{\pi}{L}\right) = \omega_k\left(\frac{\pi}{L}\right)$ to being an open path for the temporal modulation i.e., $\omega_k\left(-\frac{\pi}{L}\right) \neq \omega_k\left(\frac{\pi}{L}\right)$.

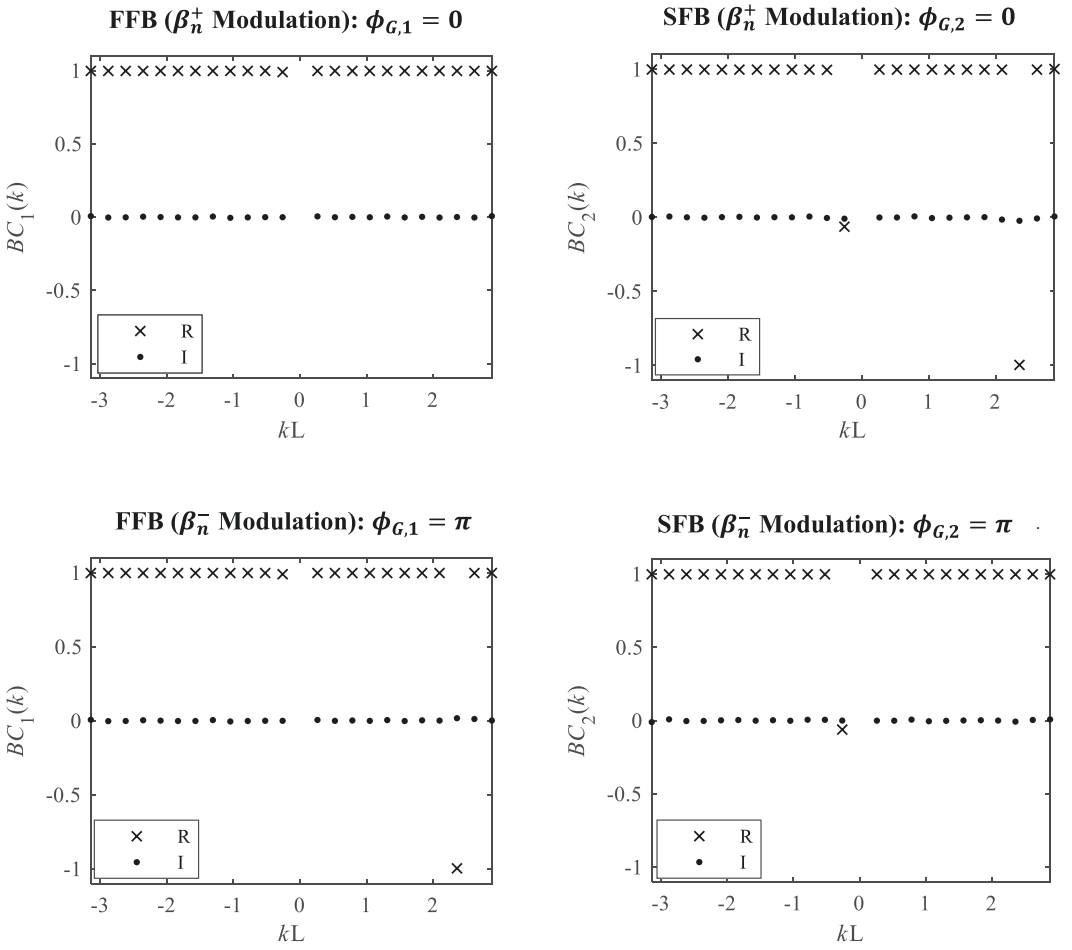

Fig. 6. Berry connection ($BC_p(k)$) and geometric phase ($\phi_{G,p}$) values at each fundamental branch p and for both modulations (R and I stand for real and imaginary components, respectively). The system is composed of 24 unit cells.

4.2. Theory of hybridization gaps

From the numerical study we have observed hybridization gaps that lead to a discontinuity in the fundamental branch amplitudes (see Figs. 3 and 4). In this section, we theoretically estimate k_{gap} and give an explanation of the discontinuity.

As mentioned in Section 3.2, the zeroth-order solution of the perturbation analysis represents propagation of an elastic wave in a homogeneous medium with the eigenvalue ω_0. However, the first-order solution (Eq. (13)) corresponds to the first-order Brillouin harmonics that is observed in the band structures of the time-dependent superlattice (see Fig. 2) [5]. If f_0 is the frequency of the elastic waves, then the frequency of the Brillouin modes (f_α) contains harmonics of the frequency associated with the moving modulation $\left(f_m = \frac{\omega_m}{2\pi}\right)$ i.e., $f_\alpha = f_0 + \alpha f_m$; $\alpha = 1, 2, \ldots$ [5]. These harmonic components appear as Stokes and anti-Stokes bands parallel to the folded bands of the static superlattice corresponds to ω_0. The scattered modes hybridize with the static folded bands to form directional band gaps i.e., opening of band gaps only on one side of the Brillouin zone. Therefore, the gaps in Figs. 2 and 7 result from the hybridization between a first-order Brillouin harmonic $(\alpha = 1)$ and the first and second zeroth-order bands of the static superlattice.

We analyze the above results using the discrete mass and spring elastic superlattice. To zeroth-order in perturbation, the dispersion relation for 1D mass-spring system is

$$\omega(k) = 2\sqrt{\frac{\beta_0}{m}}\left|\sin\left(\frac{k}{2}\right)\right| \tag{14}$$

For a superlattice of four identical masses per unit cell with no spring constants modulation, there are four folded bands. The dispersion relation for the lowest two bands is $\omega_{0,1} = 2\sqrt{\frac{\beta_0}{m}}\left|\sin\left(\frac{k}{2}\right)\right|$ and $\omega_{0,2} = 2\left|\sin\left(\frac{-|k|+\frac{2\pi}{L}}{2}\right)\right| = 2\sqrt{\frac{\beta_0}{m}}\left|\sin\left(\frac{\pi}{4} - \frac{|k|}{2}\right)\right|$, where $kL = [-\pi, \pi]$ and the subscript $(0, j)$ indicates zeroth-order modes of branch j. We know that hybridization band gaps form between the zeroth-order modes and the first Brillouin harmonics at the resonance wave numbers, k_{gap}. Therefore, the 2nd hybridization gap forms at the intersection between upper zeroth-order band $(\omega_{0,2})$ and lower first Brillouin harmonic $(\omega_{1,1})$ (see Fig. 7). The lower first Brillouin harmonic $(\omega_{1,1})$ can be obtained by shifting the zeroth-order band by $+\omega_m$ i.e., $\omega_{1,1} = \omega_{0,1} + \omega_m$. Therefore, at the hybridization wave number k_{gap} we have

$$\omega_{0,1} + \omega_m = \omega_{0,2} \Rightarrow 2\sqrt{\frac{\beta_0}{m}}\left|\sin\left(\frac{k_{gap}}{2}\right)\right| + \omega_m = 2\sqrt{\frac{\beta_0}{m}}\left|\sin\left(-\frac{k_{gap}}{2} + \frac{\pi}{4}\right)\right| \tag{15}$$

For the given modulation speed of $V_m = 350\ m/s$, we obtain $k_{gap}L = 2.472$ within the 1st Brillouin zone.

We now analyze the normalized complex amplitudes and phases of 1D mass and spring superlattice composed of four identical masses per unit cell but no spring constants modulation. In Figs. 8 and 9 we plot the normalized complex amplitudes and phases for the lowest two bands using the zeroth-order frequency spectrum ($\omega_{0,1}$ and $\omega_{0,2}$). To calculate the complex amplitudes and phases, we have used the SAAP method as discussed in Section 3.1. By comparing Figs. 8 and 9 with Figs. 3–5, we see that both the amplitudes and phases are in excellent agreement until the hybridization point, $k_{gap}L$. Therefore, using the zeroth-order solution in ε, we can theoretically calculate the complex amplitudes and phase of the two fundamental branches up to k_{gap}. To the first-order in ε, we find a change in sign of the amplitude of the first-order displacement function as the wave number is varied across k_{gap} (see Eq. (13)). This is because as we pass through k_{gap}, the wave function transitions

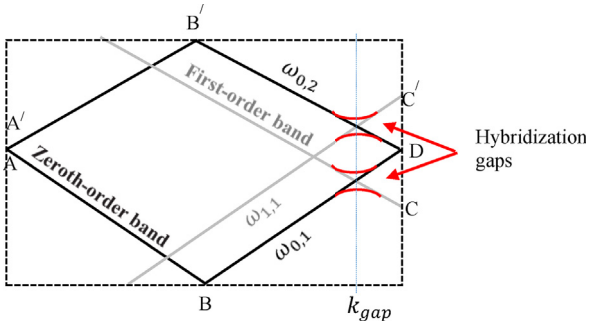

Fig. 7. Schematic illustration of the band structure of the static superlattice and of the Brillouin harmonic bands involved in the formation of the hybridization gaps.

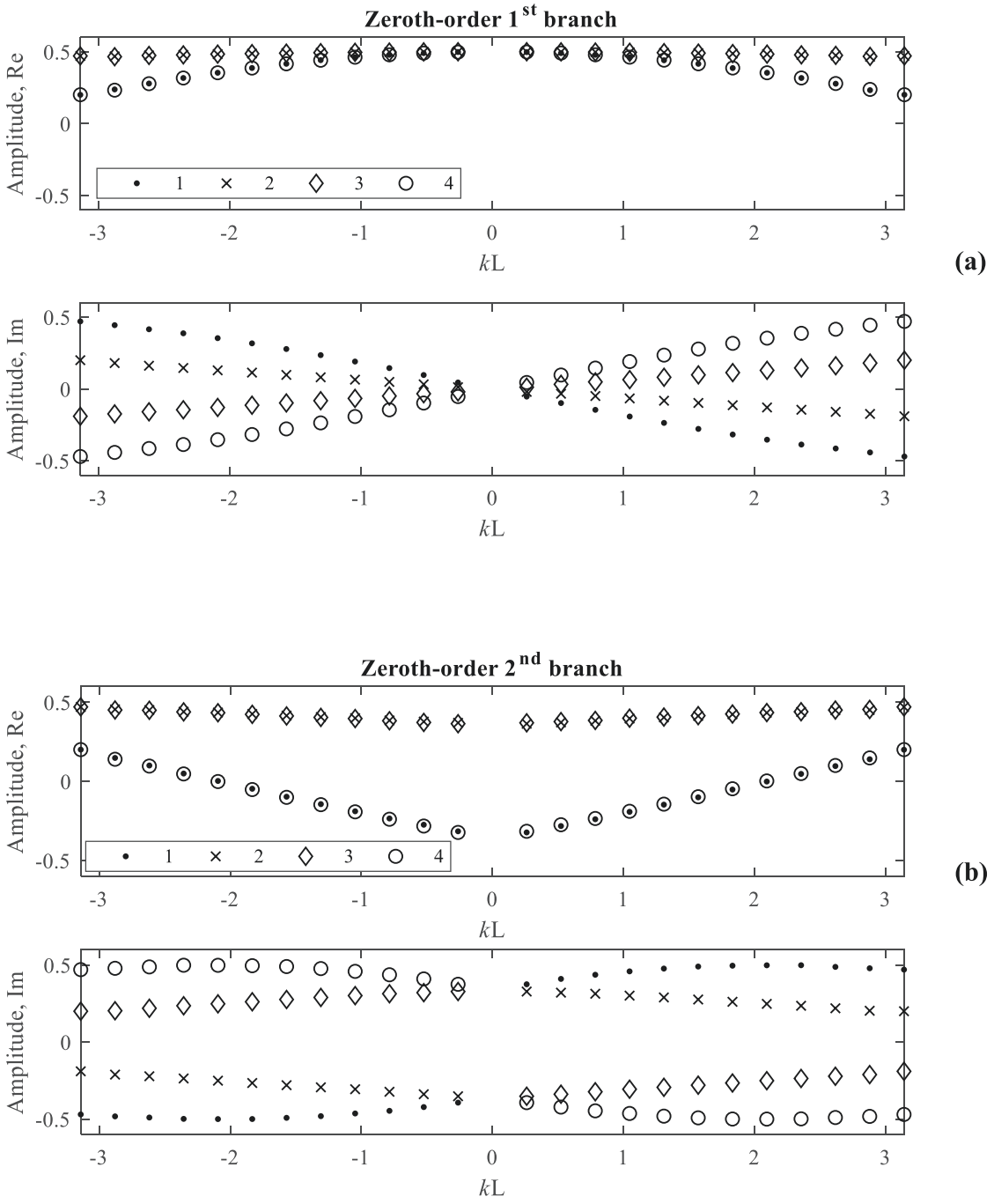

Fig. 8. Normalized complex amplitudes of zeroth-order (a) 1st ($\omega_{0,1}$) and (b) 2nd ($\omega_{0,2}$) branches of masses 1, 2, 3, and 4. The system is composed of 24 unit cells.

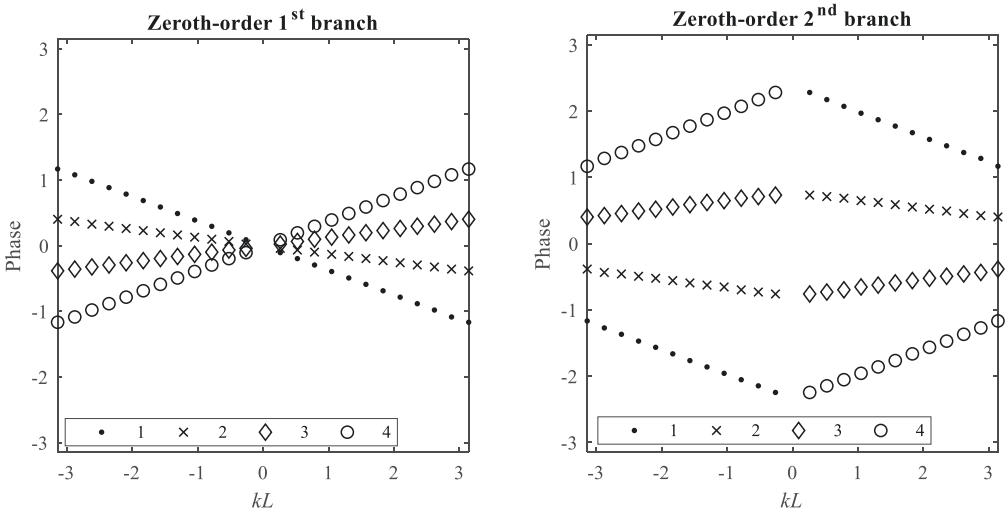

Fig. 9. Phase values of zeroth-order 1st $(\omega_{0,1})$ and 2nd $(\omega_{0,2})$ branches of masses 1, 2, 3, and 4. The system is composed of 24 unit cells.

from a state corresponding to a zeroth-order type wave $(e^{i\omega_0(k+g)\tau_0})$ to a wave having the characteristics of a first-order wave $(e^{i[\omega_0(k+g-k_m)-\omega_m]\tau_0})$. The transition between these two types of wave leads to a phase difference of π and hence a discontinuity at k_{gap}. From Fig. 7, we see that there are four transitions between these two types of waves. However, as we discuss in the next paragraph, if there is a π phase difference or discontinuity at k_{gap} to the first transitions, there is no discontinuity at the second transitions, and vice versa. These alternate discontinuity phenomenon continues to the upper pairs of transitions as well.

Let's assume $\phi(k)$ is the phase value of the zeroth-order type wave and there is a π phase difference at the first transition. Though before and after k_{gap}, the phase value of zeroth-order band will remain the same, however due to a π phase difference at the first transition, after k_{gap} the phase value of the first-order band will be $\phi(k) + \pi$. Moreover, since there is a change in sign of the amplitude of the first-order displacement function as the wave number is varied across k_{gap}, to the left of k_{gap} the phase value of the first-order band will be $\phi(k)$. Therefore, we find 0 local phase difference at the second transitions between these two types of waves. Similarly, there is π and 0 phase difference at the third and four transitions between these two types of waves, respectively. As a result, if there is a discontinuity at the 1st transition (similar to FFB of Fig. 2), there is no discontinuity at the 4th transition (similar to SFB of Fig. 3), and vice versa.

5. Conclusions

We have demonstrated using perturbation theory and numerical calculations of the SAAP method that the geometric phase of the first two fundamental branches of the band structure of a mass and spring superlattice is not changed by a temporal modulation of stiffness. However, there are two effects of temporal modulations on the band structure that have been shown here, 1) the geometric phase changes from being a closed loop to an open loop geometric phase and 2) hybridization gaps are opened in the band structure for each of the fundamental branches. Within the context of multiple time scale perturbation theory, we observe that the fundamental bands moves from the zeroth-order solution to the first-order solution at the hybridization gap wave number, k_{gap}. It is noted that at k_{gap} as the wave number increases, if there is a discontinuity in the traveling wave amplitudes when the zeroth-order solution changes to the first-order solution, there is no discontinuity when the first-order solution changes to the zeroth-order solution. In either case, the overall change to the geometric phase for each fundamental band is invariant to the temporal modulation.

The insights provided by SAAP method and multiple time scale perturbation theory can be used in understanding and designing phononic structures that support topological characteristics that may include non-reciprocal propagation of acoustic waves for a range of frequencies. These topological invariants of the geometric phase in a periodic system can also be used to determine the existence of topological interface states within a certain band gap [39]. Further, based on the invariance of geometric phase to temporal modulation, the topological character of an acoustic can be determined for the static spatial modulation. Engineering acoustic metamaterial band structures to manage both the position in wave number and width in frequency, as well as, controlling the topological character of these metamaterials can give rise of exciting new functional capabilities and applications for these remarkable structures.

The asymmetry of the elastic band structure, observed in the current work, also leads to non-reciprocity and hence in turn can lead to immunity to backscattering by any defect or imperfection in the medium. These properties readily suggest applications in the domain of elastic wave-based signal processing and in particular, the possibility of utilizing non-reciprocity to achieve low loss coherent signal propagation in many technological devices such as telecommunication surface acoustic wave (SAW) or bulk acoustic wave (BAW) filters [40]. These low loss devices would then consume significantly less power and would have significant impact on telecommunication technologies. Furthermore, we have observed that the Berry phase remains "quantized" by taking value of either π or 0. This quantization suggests that the classical elastic system investigated here may lead to analogies with true quantum mechanical systems. It is therefore possible to employ and control the Berry phase (and perhaps the geometric phase in general) to encode information similarly to that encoded in emerging quantum information storage and processing devices [41]. Our work therefore may also result in alternative paradigm in quantum-analogue information processing. Finally, the geometrical phase investigated here is a non-local quantity as it represents the collective behavior of a number of spatially distributed elastic masses. The extension to heterogeneous continuum media is straightforward and the geometrical phase would be a measure of the global spatial (also temporal) variations in the properties of the medium. In that sense, the geometrical phase represents the collective effect of scattering by the heterogeneities in the medium. Our work suggest therefore that the geometrical phase and the Berry phase may be used in ultrasonic or acoustic sensing of infrastructure [42].

Acknowledgements

This work was supported by National Science Foundation award EFRI # 1640860.

Appendix

A1. Geometric/Berry phase and topology

In this appendix, we illustrate the concept of topology for elastic waves in the mass and spring superlattice. The topological characteristics of waves in elastic structures are determined by the geometric/Berry phase of waves, as a characterization of the global vibrational behavior of the system.

As a demonstration, we consider a system of two identical masses per unit cell with spring constants modulation [29]. The equations of motion for masses 1 and 2 of the N_i-th unit cell interacting with spring constants β_1 and β_2 in an infinite 1D system are (see Fig. A1)

$$\begin{aligned} m\ddot{u}_{1,N_i}(t) &= \beta_2\left[u_{2,N_i-1}(t) - u_{1,N_i}(t)\right] - \beta_1\left[u_{1,N_i}(t) - u_{2,N_i}(t)\right], \\ m\ddot{u}_{2,N_i}(t) &= \beta_1\left[u_{1,N_i}(t) - u_{2,N_i}(t)\right] - \beta_2\left[u_{2,N_i}(t) - u_{1,N_i+1}(t)\right] \end{aligned} \tag{A1}$$

In Eq. (A1), m is the mass, β_1 and β_2 are the force constants of the spring, and t is time, respectively. The dot denotes differentiation with respect to time.

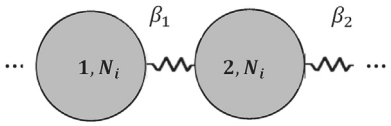

Fig. A1. Schematic illustration of a 1D chain comprised of two mass unit cells and springs with spatial stiffness modulations.

We seek traveling wave solutions of Eq. (A1) using the following ansatz [29]:

$$u_{1,N_i}(t) = A_1 e^{ikN_iL + i\omega t} \text{ and } u_{2,N_i}(t) = A_2 e^{ikN_iL + i\omega t}, \tag{A2}$$

which, as anticipated in connection to the Berry phase calculation, have amplitudes A_n that are periodic in reciprocal space. Substituting Eq. (A2) to Eq. (A1) leads to

$$\begin{pmatrix} \alpha & -\gamma \\ -\gamma^* & \alpha \end{pmatrix} \begin{pmatrix} A_1 \\ A_2 \end{pmatrix} = \begin{pmatrix} 0 \\ 0 \end{pmatrix}, \tag{A3}$$

with $(\beta_1 + \beta_2\, e^{-ikL}) = \gamma$ and $(\beta_1 + \beta_2\ - m\omega^2) = \alpha$ Taking the complex conjugate of Eq. (A3) and exchanging rows and columns, we have

$$\begin{pmatrix} \alpha & -\gamma \\ -\gamma^* & \alpha \end{pmatrix} \begin{pmatrix} A_2^* \\ A_1^* \end{pmatrix} = \begin{pmatrix} 0 \\ 0 \end{pmatrix} \tag{A4}$$

Comparing Eqs. (A3) and (A4) we find that each is satisfied if

$$A_1 = A_2^* \tag{A5}$$

Further, from Eq. (A3) we obtain the dispersion relation

$$\omega_k^2 = \frac{1}{m}\left(\beta_1 + \beta_2 \mp \sqrt{(\beta_1 + \beta_2)^2 - 4\beta_1\beta_2 \sin^2\left(\frac{kL}{2}\right)}\right); \tag{A6}$$

where the first sign corresponds to the acoustic branch and the second sign corresponds to the optical branch in the band structure. Choosing these solutions for the frequencies, we have for the amplitudes:

$$\frac{A_1}{A_2} = \pm\frac{\sqrt{\gamma}}{\sqrt{\gamma^*}} \tag{A7}$$

Taking into account Eq. (A5) leads to the following selection for the amplitudes of the acoustic branch

$$A_{1,1} = \sqrt{\gamma}, \quad A_{2,1} = \sqrt{\gamma^*}, \tag{A8}$$

since for the acoustic branch $\frac{A_{1,1}}{A_{2,1}} = \frac{\sqrt{\gamma}}{\sqrt{\gamma^*}}$. For the optical branch

$$A_{1,2} = \sqrt{e^{-i\pi}\,\gamma}, \quad A_{2,2} = \sqrt{e^{i\pi}\gamma^*}, \tag{A9}$$

which satisfies Eq. (A7) taking the minus sign.

In Fig. A2, we plot a representation of the manifold spanned by the real and imaginary parts of the amplitude unit vector, $\vec{\tilde{A}}$ (calculated using Eq. (10)), within the Brillouin zone. At each k point, mapped on to the angle to form a ring, we have an arrow pointing in the $\vec{\tilde{A}}$ direction (red arrow: k varies from $-\pi/L$ to 0; blue arrow: k varies from 0 to π/L). We take $\tilde{A}_{2,j}(k)$ along the normal to the ring plane and $\tilde{A}_{1,j}(k)$ along the radius with the positive direction pointing away from the center of the ring. As $A_1 = A_2^*$ (Eq. (A5)), the $\vec{\tilde{A}} = (\tilde{A}_{1,j}(k), \tilde{A}_{2,j}(k))$ vectors form a 45° angle with the normal to the ring plane, and hence there exists only twists but not a change in the direction of $\vec{\tilde{A}}$. Moreover, the amplitude unit vector for $\beta_1/\beta_2 = 0.5$ generates a manifold with the imaginary part taking the form of a closed ribbon with a single twist at $k = 0$ (see Fig. A2b). The total accumulated geometric phase over the Brillouin zone is therefore π. In contrast, the amplitude unit vector for $\beta_1/\beta_2 = 2$ generates a manifold with the imaginary part taking the form of a closed ribbon with two twists at $k = 0$ and at the boundaries of the Brillouin zone (see Fig. A2a). The total accumulated geometric phase over the Brillouin zone is therefore zero. These two manifolds differ in their topology by one twist.

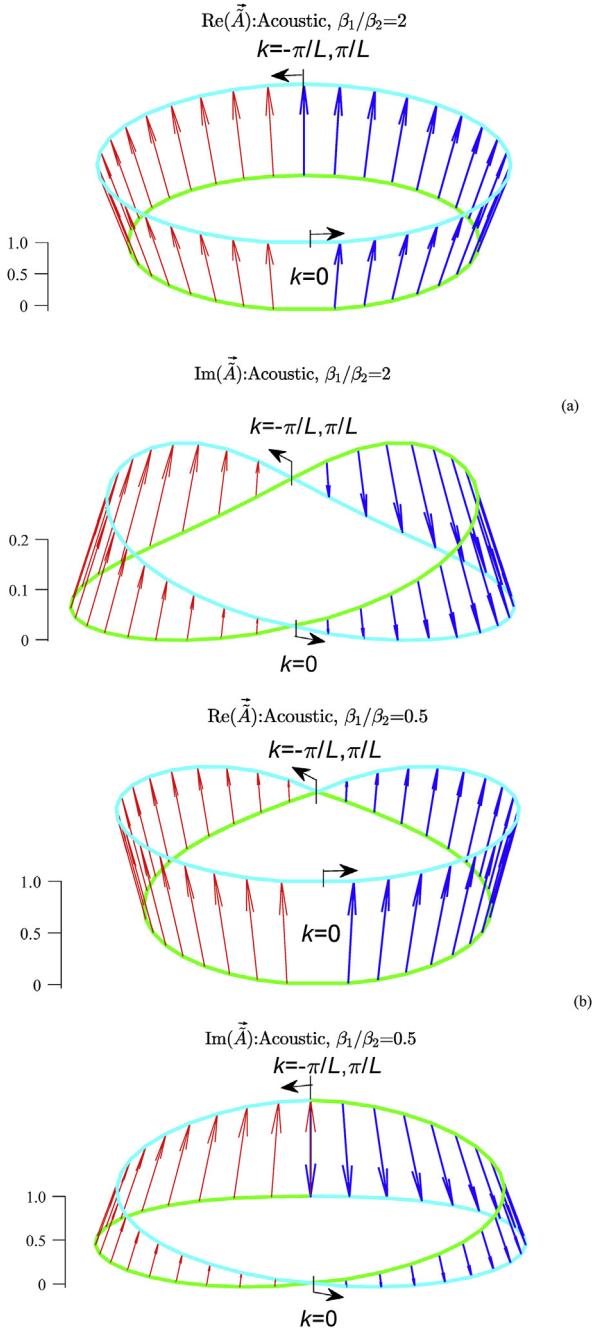

Fig. A2. Analytical results for the real (Re) and imaginary (Im) representation of the manifold generated by the evolution of the amplitude unit vector $\vec{A}$ along the path in the Brillouin zone from $k = -\pi/L$ to 0 (red arrow) and from $k = 0$ to π/L (blue arrow). Two cases are showed: (a) with $\beta_1/\beta_2 = 2$ and (b) with $\beta_1/\beta_2 = 0.5$. The scale represents the magnitude of the amplitude unit vector $\vec{A}$. The vertical elevation of the viewpoint of the manifold is 45°. The system is composed of 36 unit cells.

References

[1] P. Deymier, K. Runge, Sound Topology, Duality, Coherence and Wave-Mixing: an Introduction to the Emerging New Science of Sound, Springer International Publishing, 2017. https://www.springer.com/us/book/9783319623795. (Accessed 11 July 2018).
[2] P.A. Deymier, K. Runge, N. Swinteck, K. Muralidharan, Torsional topology and fermion-like behavior of elastic waves in phononic structures, Compt. Rendus Mec. 343 (2015) 700–711, https://doi.org/10.1016/j.crme.2015.07.003.
[3] P.A. Deymier, K. Runge, N. Swinteck, K. Muralidharan, Rotational modes in a phononic crystal with fermion-like behavior, J. Appl. Phys. 115 (2014) 163510, https://doi.org/10.1063/1.4872142.
[4] N. Swinteck, S. Matsuo, K. Runge, J.O. Vasseur, P. Lucas, P.A. Deymier, Bulk elastic waves with unidirectional backscattering-immune topological states in a time-dependent superlattice, J. Appl. Phys. 118 (2015) 063103, https://doi.org/10.1063/1.4928619.

[5] P.A. Deymier, V. Gole, P. Lucas, J.O. Vasseur, K. Runge, Tailoring phonon band structures with broken symmetry by shaping spatiotemporal modulations of stiffness in a one-dimensional elastic waveguide, Phys. Rev. B. 96 (2017) 064304, https://doi.org/10.1103/PhysRevB.96.064304.
[6] C. Croënne, J.O. Vasseur, O. Bou Matar, M.-F. Ponge, P.A. Deymier, A.-C. Hladky-Hennion, B. Dubus, Brillouin scattering-like effect and non-reciprocal propagation of elastic waves due to spatio-temporal modulation of electrical boundary conditions in piezoelectric media, Appl. Phys. Lett. 110 (2017) 061901, https://doi.org/10.1063/1.4975680.
[7] G. Trainiti, M. Ruzzene, Non-reciprocal elastic wave propagation in spatiotemporal periodic structures, New J. Phys. 18 (2016) 083047, https://doi.org/10.1088/1367-2630/18/8/083047.
[8] H. Nassar, X.C. Xu, A.N. Norris, G.L. Huang, Modulated phononic crystals: non-reciprocal wave propagation and Willis materials, J. Mech. Phys. Solids 101 (2017) 10–29, https://doi.org/10.1016/j.jmps.2017.01.010.
[9] H. Nassar, H. Chen, A.N. Norris, G.L. Huang, Non-reciprocal flexural wave propagation in a modulated metabeam, Extreme Mech. Lett. 15 (2017) 97–102, https://doi.org/10.1016/j.eml.2017.07.001.
[10] P. Deymier, K. Runge, One-dimensional mass-spring chains supporting elastic waves with non-conventional topology, Crystals 6 (2016) 44, https://doi.org/10.3390/cryst6040044.
[11] J.H. Hannay, Angle variable holonomy in adiabatic excursion of an integrable Hamiltonian, J. Phys. Math. Gen. 18 (1985) 221, https://doi.org/10.1088/0305-4470/18/2/011.
[12] C.A. Mead, The geometric phase in molecular systems, Rev. Mod. Phys. 64 (1992) 51–85, https://doi.org/10.1103/RevModPhys.64.51.
[13] M. Atala, M. Aidelsburger, J.T. Barreiro, D. Abanin, T. Kitagawa, E. Demler, I. Bloch, Direct measurement of the Zak phase in topological Bloch bands, Nat. Phys. 9 (2013) 795–800, https://doi.org/10.1038/nphys2790.
[14] G. Jotzu, M. Messer, R. Desbuquois, M. Lebrat, T. Uehlinger, D. Greif, T. Esslinger, Experimental realization of the topological Haldane model with ultracold fermions, Nature 515 (2014) 237–240, https://doi.org/10.1038/nature13915.
[15] J.M. Zeuner, M.C. Rechtsman, Y. Plotnik, Y. Lumer, M.S. Rudner, M. Segev, A. Szameit, Probing topological invariants in the bulk of a non-Hermitian optical system, Phys. Rev. Lett. 115 (2015), https://doi.org/10.1103/PhysRevLett.115.040402.
[16] S. Longhi, Zak phase of photons in optical waveguide lattices, Opt. Lett. 38 (2013) 3716–3719, https://doi.org/10.1364/OL.38.003716.
[17] M. Xiao, G. Ma, Z. Yang, P. Sheng, Z.Q. Zhang, C.T. Chan, Geometric phase and band inversion in periodic acoustic systems, Nat. Phys. 11 (2015) 240–244, https://doi.org/10.1038/nphys3228.
[18] R.K. Pal, M. Ruzzene, Edge waves in plates with resonators: an elastic analogue of the quantum valley Hall effect, New J. Phys. 19 (2017) 025001, https://doi.org/10.1088/1367-2630/aa56a2.
[19] P.A. Deymier, K. Runge, J.O. Vasseur, Geometric phase and topology of elastic oscillations and vibrations in model systems: harmonic oscillator and superlattice, AIP Adv. 6 (2016) 121801, https://doi.org/10.1063/1.4968608.
[20] S. Wang, G. Ma, C.T. Chan, Topological transport of sound mediated by spin-redirection geometric phase, Sci. Adv. 4 (2018), https://doi.org/10.1126/sciadv.aaq1475 eaaq1475.
[21] A.B. Khanikaev, R. Fleury, S.H. Mousavi, A. Alù, Topologically robust sound propagation in an angular-momentum-biased graphene-like resonator lattice, Nat. Commun. 6 (2015) 8260, https://doi.org/10.1038/ncomms9260.
[22] G. Salerno, T. Ozawa, H.M. Price, I. Carusotto, Floquet topological system based on frequency-modulated classical coupled harmonic oscillators, Phys. Rev. B. 93 (2016) 085105, https://doi.org/10.1103/PhysRevB.93.085105.
[23] J. Paulose, A.S. Meeussen, V. Vitelli, Selective buckling via states of self-stress in topological metamaterials, Proc. Natl. Acad. Sci. 112 (2015) 7639–7644, https://doi.org/10.1073/pnas.1502939112.
[24] L.M. Nash, D. Kleckner, A. Read, V. Vitelli, A.M. Turner, W.T.M. Irvine, Topological mechanics of gyroscopic metamaterials, Proc. Natl. Acad. Sci. 112 (2015) 14495–14500, https://doi.org/10.1073/pnas.1507413112.
[25] P. Wang, L. Lu, K. Bertoldi, Topological phononic crystals with one-way elastic edge waves, Phys. Rev. Lett. 115 (2015) 104302, https://doi.org/10.1103/PhysRevLett.115.104302.
[26] Z. Yang, F. Gao, X. Shi, X. Lin, Z. Gao, Y. Chong, B. Zhang, Topological acoustics, Phys. Rev. Lett. 114 (2015) 114301, https://doi.org/10.1103/PhysRevLett.114.114301.
[27] M.V. Berry, Quantal phase factors accompanying adiabatic changes, Proc. R. Soc. Lond. 392 (1984) 45–57, https://doi.org/10.1098/rspa.1984.0023.
[28] J. Samuel, R. Bhandari, General setting for Berry's phase, Phys. Rev. Lett. 60 (1988) 2339–2342, https://doi.org/10.1103/PhysRevLett.60.2339.
[29] M.A. Hasan, L. Calderin, P. Lucas, K. Runge, P.A. Deymier, Spectral analysis of amplitudes and phases of elastic waves: application to topological elasticity, J. Acoust. Soc. Am. 146 (1) (2019) (accepted).
[30] E.S. Cassedy, A.A. Oliner, Dispersion relations in time-space periodic media: Part I—stable interactions, Proc. IEEE 51 (1963) 1342–1359, https://doi.org/10.1109/PROC.1963.2566.
[31] J. Gump, I. Finkler, H. Xia, R. Sooryakumar, W.J. Bresser, P. Boolchand, Light-induced giant softening of network glasses observed near the mean-field rigidity transition, Phys. Rev. Lett. 92 (2004) 245501, https://doi.org/10.1103/PhysRevLett.92.245501.
[32] R. Resta, Manifestations of Berry's phase in molecules and condensed matter, J. Phys. Condens. Matter 12 (2000) R107, https://doi.org/10.1088/0953-8984/12/9/201.
[33] J. Zak, Berry's phase for energy bands in solids, Phys. Rev. Lett. 62 (1989) 2747–2750, https://doi.org/10.1103/PhysRevLett.62.2747.
[34] I.C. Khoo, Y.K. Wang, Multiple time scale analysis of an anharmonic crystal, J. Math. Phys. 17 (1976) 222–227, https://doi.org/10.1063/1.522884.
[35] H. Nassar, H. Chen, A.N. Norris, M.R. Haberman, G.L. Huang, Non-reciprocal wave propagation in modulated elastic metamaterials, Proc. R. Soc. A 473 (2017) 20170188, https://doi.org/10.1098/rspa.2017.0188.
[36] J. Vila, R.K. Pal, M. Ruzzene, G. Trainiti, A Bloch-based procedure for dispersion analysis of lattices with periodic time-varying properties, J. Sound Vib. 406 (2017) 363–377, https://doi.org/10.1016/j.jsv.2017.06.011.
[37] E.J. Reed, M. Soljačić, J.D. Joannopoulos, Color of shock waves in photonic crystals, Phys. Rev. Lett. 90 (2003) 203904, https://doi.org/10.1103/PhysRevLett.90.203904.
[38] F. Cai, Z. He, A. Zhang, Y. Ding, Z. Liu, Anomalous Doppler effects in bulk phononic crystal, Phys. Lett. A 374 (2010) 3971–3976, https://doi.org/10.1016/j.physleta.2010.07.045.
[39] Y. Meng, X. Wu, R.-Y. Zhang, X. Li, P. Hu, L. Ge, Y. Huang, H. Xiang, D. Han, S. Wang, W. Wen, Designing topological interface states in phononic crystals based on the full phase diagrams, New J. Phys. 20 (2018) 073032, https://doi.org/10.1088/1367-2630/aad136.
[40] K.-Y. Hashimoto, Surface Acoustic Wave Devices in Telecommunications: Modelling and Simulation, Springer-Verlag, Berlin Heidelberg, 2000. https://www.springer.com/us/book/9783540672326. (Accessed 3 January 2019).
[41] A. Ekert, M. Ericsson, P. Hayden, H. Inamori, J.A. Jones, D.K.L. Oi, V. Vedral, Geometric quantum computation, J. Mod. Opt. 47 (2000) 2501–2513, https://doi.org/10.1080/09500340008232177.
[42] M.I. Faley, E.A. Kostyurina, K.V. Kalashnikov, Y.V. Maslennikov, V.P. Koshelets, R.E. Dunin-Borkowski, Superconducting quantum interferometers for nondestructive evaluation, Sensors 17 (2017) 2798, https://doi.org/10.3390/s17122798.